Investigation of Ti/Au Transition-Edge Sensors for Single-Photon Detection

(Article begins on next page)

Investigation of Ti/Au Transition-Edge Sensors for Single-Photon Detection

Xiaolong Xu[1] · Mauro Rajteri[2] · Jinjin Li[1] · Shuo Zhang[3] · Carlo Pepe[2,4] ·
Jian Chen[1] · Huifang Gao[1] · Qi Li[1] · Wei Li[1] · Xu Li[1] · Mingyu Zhang[1] ·
Yanyan Ouyang[1] · Xueshen Wang[1]

Abstract

Transition-edge sensors (TES) are remarkable superconducting devices for a wide range of radiation detection with the ability of both energy resolution and counting photons. For the detection of single photons at telecom wavelength, optical Ti/Au bilayer TESs are fabricated and characterized. The superconducting transition temperature (T_c) of the Ti/Au films is effectively tuned from 162 to 72 mK by increasing the relative thickness ratio between the Au and Ti layer. The sensitive area is 20 µm × 20 µm, on which an SiO_2/SiN_x antireflection structure is coated by an ICP-PECVD process. The TES device shows an energy resolution of 0.19 eV and can discriminate up to 36 incident photons, with an effective time constant around 107 µs at 95 mK.

Keywords Superconducting transition-edge sensors · Ti/Au bilayer · Antireflection coating

1 Introduction

Superconducting transition-edge sensors (TESs) have been widely used for single-photon detection from near-infrared, visible light, X-ray to even γ-ray. The most distinctive feature of TESs is the single-photon energy resolution and the photon number resolving (PNR) capability (when the photon energy is already known) [1],

✉ Xueshen Wang
  wangxs@nim.ac.cn

1 National Institute of Metrology (NIM), Beijing 100029, China

2 Istituto Nazionale di Ricerca Metrologica (INRiM), 10135 Turin, Italy

3 ShanghaiTech University, Shanghai 201210, China

4 Politecnico di Torino, 10129 Turin, Italy

but they also show high quantum efficiency [2], negligible dark counts [3] and show great potential in quantum information [4], dark matter detection [5], X-ray free-electron laser [6], satellite X-ray observatory [7] and cosmic microwave background observatory [8]. In the field of optical metrology, TESs will realize the quantum revolution of photometry [9].

In this paper, we report about the fabrication and preliminary characterization of optical Ti/Au TESs for single-photon detection at telecom wavelength. The critical temperature T_c of Ti/Au superconducting films is tuned by controlling the thickness ratio of the two layers. An antireflection SiO_2/SiN_x coating is deposited on the Ti/Au bilayer film before the alignment of an optical fiber, and the simulated reflectivity is shown. The TES device shows a high energy resolution (0.19 eV) and PNR capability up to 36 photons.

2 TESs Fabrication

NIM fabricated TESs with two active areas (10 μm×10 μm and 20 μm×20 μm) on the wafer. Considering the reliability of the optical fiber alignment to avoid optical geometric loss, we present preliminary results for the TES with 20 μm×20 μm active area, which allows an easier and better fiber optics alignment, but with a larger heat capacity that affects the energy resolution. We have confirmed that the 20 μm×20 μm Ti/Au TES has sufficient ability to resolve 1550-nm single-photon detection.
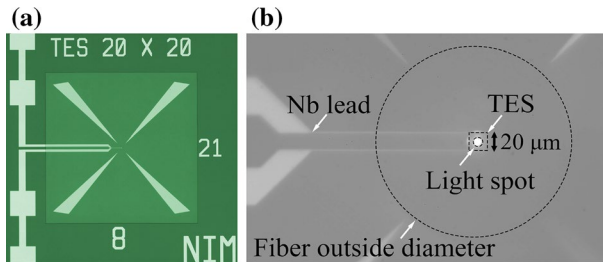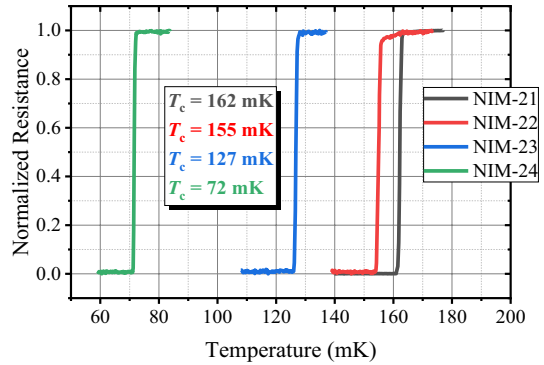
2.1 Ti/Au Bilayer Films

The Ti/Au bilayer films are deposited on double-polished 3-inch 500-μm silicon substrates with 500-nm SiN_x layers on both sides using a magnetron sputtering process. The base pressure is $\sim 10^{-6}$ Pa, and the sputtering pressure is 0.1 Pa. Firstly, a 5-nm Ti film is sputtered as the adhesion layer. Then an Au layer is deposited as the normal metal layer with a thickness d_{Au} of 60 nm. A variable thickness d_{Ti} of Ti layer (40 to 70 nm) is deposited on Au layer.

The effective resistivity ρ_{eff}, root-mean-square roughness R_q, and T_c of the Ti/Au bilayer are measured for different d_{Ti}/d_{Au} ratios. The ρ_{eff} is defined as $R\square \times (d_{Au} + d_{Ti})$, where $R\square$ is the sheet resistance. The ρ_{eff} is proportional to the ratio d_{Ti}/d_{Au} as shown in Tab.1. NIM-21 shows the highest $\rho_{eff} = 76$ $n\Omega\cdot m$, and

Table 1 The ρ_{eff} and R_q of Ti/Au films

Sample	Thickness/nm		ρ_{eff} /nΩ·m	R_q /nm
	Ti	Au		
NIM-21	70	60	76	1.11
NIM-22	60	60	65	1.02
NIM-23	50	60	57	1.04
NIM-24	40	60	53	1.01

Fig. 1 The Tc of the Ti/Au bilayers with different dTi/dAu ratios (Color figure online)

T_c = 162 mK
T_c = 155 mK
T_c = 127 mK
T_c = 72 mK

NIM-21
NIM-22
NIM-23
NIM-24

(a) TES 20 X 20
21
8 NIM

(b) Nb lead
TES
20 μm
Light spot
Fiber outside diameter

Fig. 2 Images of an optical Ti/Au TES with a 20 μm×20 μm sensitive area with Nb leads: **a** a whole view of the TES device; **b** the enlarged view of the device achieved during the optical fiber alignment process. A light spot can be observed at the center of TES to locate the position of optical fiber (Color figure online)

NIM-24 shows the lowest ρ_{eff} as 53 $n\Omega\cdot m$, which trends to the bulk Au resistivity ~ 22 $n\Omega\cdot m$ [10]. The ρ_{eff} will be helpful for the resistance design of the TESs. The R_q is similar ~ 1 nm, indicating a good interface morphology between the Ti and Au layers. The smooth interface will make weak proximity effect [11, 12].

The T_c is measured in an adiabatic demagnetization refrigerator (ADR) system with a base temperature ~ 30 mK and is shown in Fig. 1. The weak proximity effect occurs for the largest d_{Ti}/d_{Au} ratio, and the T_c of NIM-21 is 162 mK. Inversely, NIM-24 shows a stronger proximity effect which suppresses the T_c to 72 mK.

2.2 Ti/Au TESs

The optical image TES device is shown in Fig. 2. The 20 μm×20 μm active Ti/Au film area is defined by UV lithography followed by a lift-off process. The Nb superconducting leads for electrical wiring are also fabricated via a lift-off process. The

thickness of the Nb layer should be thick enough to maintain its superconductivity after the following fabrication steps.

2.3 Antireflection Structure

An antireflection structure composed of SiO_2 and SiN_x dielectric layers is deposited on the TES devices to reduce the device reflectivity. The vertical stack structure is shown in Fig. 3(a). The SiO_2 and SiN_x layers are fabricated using an inductively coupled plasma-assisted plasma-enhanced chemical vapor deposition (ICP-PECVD) method. The refractive index and extinction coefficient (n, k) are (1.47, 0), (1.92, 0), (4.03, 3.81), (0.56, 9.91) for SiO_2, SiN_x, Ti, and Au at 1550 nm, respectively. These optical parameters were measured using a Horiba UVISEL2 spectroscopic ellipsometers. The refractive index of the UV resin for the fiber alignment process (n=1.56) is similar to that of the fiber core (n=1.47) [2]. With the above parameters, the reflectivity at 1550 nm is simulated and shown in Fig. 3(b). The lowest reflectivity is near 23%. The simulated transmittance is 10^{-3}. To control the thickness accurately by the end-point detection module of ICP-PECVD, 270-nm SiO_2 and 350-nm SiN_x are deposited on the TES device.

2.4 Optical Fiber Alignment

The optical fiber alignment process is operated with an inverted optical microscope with a near-infrared CCD. The TES device is fixed on the sample holder, and the optical fiber is aligned perpendicular to the device by a six-dimension adjustment frame. Figure 2b shows the backside image captured from the CCD. As the pig-tail optical fiber is connected to a 1550-nm light source, the fiber core emits a light spot. When the light spot locates at the center of the TES, the resin is cured with UV light to fix the fiber to the device.
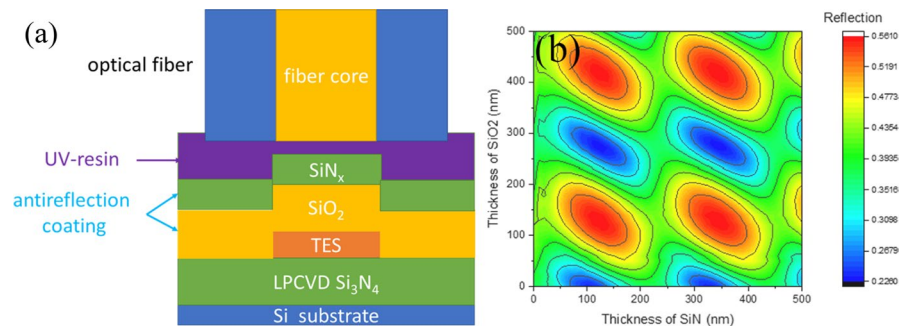
Fig. 3 a The cross section of the layer structure of the TES including the coupled optical fiber; b simulation results of the reflectivity of the optical structure (Color figure online)
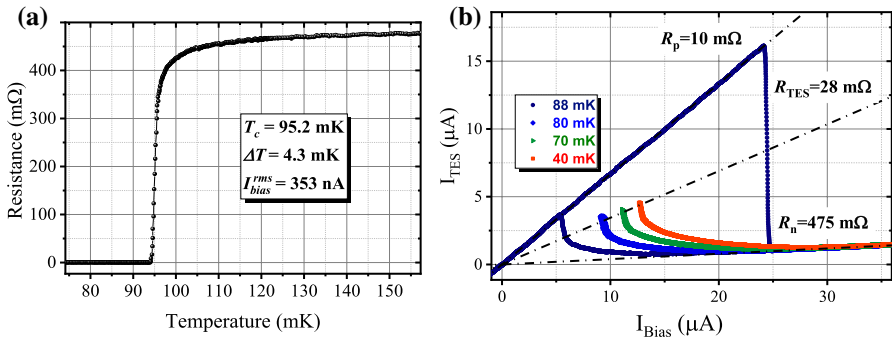
Fig. 4 **a** The Tc of the TES device vs. temperature measured with a DC-SQUID, **b** ITES vs. IBias at different base temperatures (Color figure online)

3 TES Characterization

The NIM-23 device shows a T_c of 95.2 mK in the voltage-biased circuit with a DC-SQUID (Fig. 4(a)). The TES's T_c in constant voltage mode shows around 30 mK shift compared with the film shown in Fig. 1. The device shows a sharp superconducting transition with a width $\Delta T = 4.3$ mK. The TES working point is around 6% of R_n.

Figure 4(b) shows the current flowing through TES I_{TES} as a function of I_{Bias} for the bath temperature T_b from 40 to 88 mK. The 20-mΩ shunt resistance R_s on the SQUID chip is selected. From the I_{TES}-I_{Bias} curves, the parasitic resistance $R_p = 10$ mΩ, the normal resistance of TES $R_n = 475$ mΩ and the working point resistance of TES $R_o = 28$ mΩ at 6% of R_n can be obtained. The heat capacity C of the Ti/Au bilayer is calculated as 2.2 fJ/K [13].

The photon detection properties are characterized with a pulsed laser at 1550 nm. With the statistics data of the pulse signals of photons detected by the TES device, the histograms of photon states are shown in Fig. 5(a) and (b). The energy resolution ΔE is defined as the full width at half maximum (FWHM) of the first photon state peak. Figure 5(a) shows the count histogram for the pulses filtered with a Wiener filter [14]. The fit of the histogram with Gaussians convoluted with a Poissonian statistics (typical of lasers) gives a detected mean photon number $\mu = 0.6$ photons per pulse and an energy resolution $\Delta E = 0.19$ eV. In the same experimental conditions, we have also continuously reduced the attenuation of the laser during the acquisition, obtaining the histogram of Fig. 5(b). In this case our TES can clearly distinguish up to 36 photons before reaching the saturation region. The typical averaged pulse response is shown in Fig. 5(c), which is fitted by a double exponential equation. The electrical time constant ($\tau_{eletrical}$) is about 360 ns. And the response time constant (τ_{eff}) is about 107 μs.
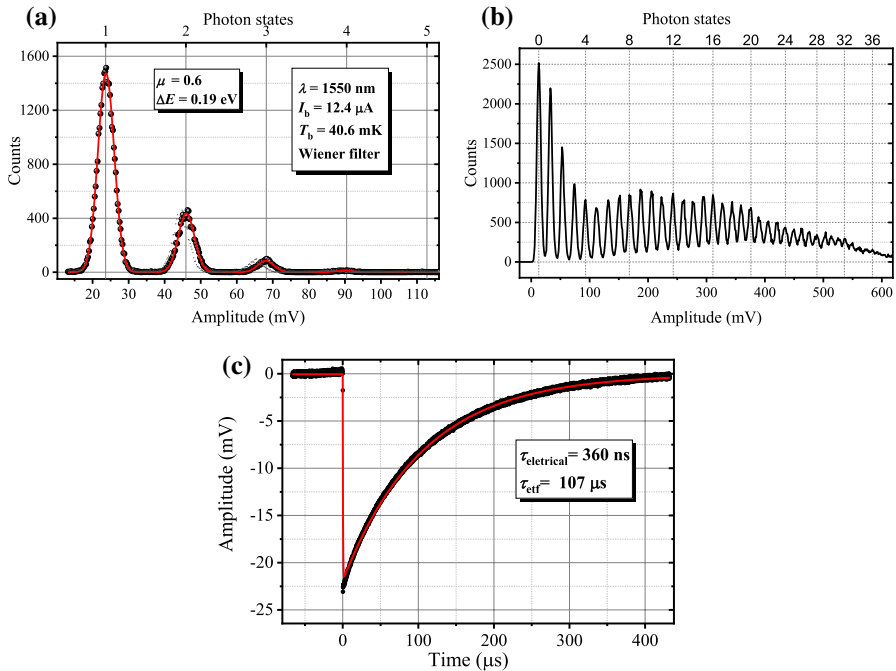
Fig. 5 Histograms of pulse height and photon states. The measurement conditions are reported in the insets. **a** The histogram is obtained from waveforms filtered with Wiener filter. The red curve is a fit with Gaussians convoluted with a Poissonian statistic; **b** the histogram is obtained directly with the signal acquired with a digital oscilloscope, while the attenuation of the laser is reduced to show the whole photon states detectable with the TES; **c** single-photon pulse response (Color figure online)

4 Conclusions

The optical Ti/Au bilayer TES device shows an energy resolution of 0.19 eV with a $20 \times 20~\mu m^2$ active area. The devices can discriminate up to 36 photon states. The results have shown that TESs are promising detectors for counting single photon and promote the application of TES on the optical quantum metrology. In the future, the quantum efficiency will be evaluated and improved by optimal optical cavity.

References

1. L. Lolli, E. Taralli, M. Rajteri, J. Low Temp. Phys. **167**, 803 (2012). https://doi.org/10.1007/s10909-012-0473-2
2. D. Fukuda et al., Opt. Express **19**, 870 (2011). https://doi.org/10.1364/OE.19.000870

3. A.J. Miller, S.W. Nam, J.M. Martinis, A.V. Sergienko, Appl. Phys. Lett. **83**, 791 (2003). https://doi.org/10.1063/1.1596723
4. R.H. Hadfield, Nat. Photonics **3**, 696 (2009). https://doi.org/10.1038/nphoton.2009.230
5. F. Paolucci et al., J. Appl. Phys. **128**, 194502 (2020). https://doi.org/10.1063/5.0021996
6. D. Li et al., J. Low Temp. Phys. **193**, 1287 (2018). https://doi.org/10.1007/s10909-018-2053-6
7. K. Nagayoshi et al., J. Low Temp. Phys. **199**, 943 (2020). https://doi.org/10.1007/s10909-019-02282-8
8. J.R. Stevens et al., J. Low Temp. Phys. **199**, 672 (2020). https://doi.org/10.1007/s10909-020-02375-9
9. J.C. Zwinkels, E. Ikonen, N.P. Fox, G. Ulm, M.L. Rastello, Metrologia **47**, R15 (2010). https://doi.org/10.1088/0026-1394/47/5/R01
10. G. Kästle et al., Phys. Rev. B **70**, 165414 (2004). https://doi.org/10.1103/PhysRevB.70.165414
11. K. Kengo et al., J. Low Temp. Phys. **193**, 349 (2018). https://doi.org/10.1007/s10909-018-1995-z
12. X. Xu et al., Nanomaterials **11**, 39 (2021). https://doi.org/10.3390/nano11010039
13. M Rajteri et al (2009) Metrologia https://doi.org/10.1088/0026-1394/46/4/S28.
14. D. Alberto et al., IEEE Trans. Appl. Supercond. **21**, 285 (2011). https://doi.org/10.1109/TASC.2010.2087736